Materials Chemistry and Physics 299 (2023) 127528

Contents lists available at ScienceDirect

Materials Chemistry and Physics

journal homepage: www.elsevier.com/locate/matchemphys

Exploration of photovoltaic behavior of fused triphenylamine moiety as core donor with modified acceptors: Star-shaped D-π-A conjugated systems

Muhammad Khalid [a,b,**], Ume Habiba Ishaque [a,b], Muhammad Adnan Asghar [c], Muhammad Adeel [d], Mohammed Mujahid Alam [e], Muhammad Imran [e], Rabia Baby [f], Ataualpa A.C. Braga [g], Muhammad Fayyaz ur Rehman [h], Muhammad Safwan Akram [i,j,*]

[a] Institute of Chemistry, Khwaja Fareed University of Engineering & Information Technology, Rahim Yar Khan, 64200, Pakistan
[b] Centre for Theoretical and -Computational Research, Khwaja Fareed University of Engineering & Information Technology, Rahim Yar Khan, 64200, Pakistan
[c] Department of Chemistry, Division of Science and Technology, University of Education Lahore, Pakistan
[d] Institute of Chemical Sciences, Gomal University, Dera Ismail Khan, Khyber Pukhtoon Khwa, Pakistan
[e] Department of Chemistry, Faculty of Science, King Khalid University, P.O. Box 9004, Abha, 61413, Saudi Arabia
[f] Department of Education, Sukkur IBA University, zip code. 65200, Pakistan
[g] Departamento de Química Fundamental, Instituto de Química, Universidade de São Paulo, Av. Prof. Lineu Prestes, 748, São Paulo, 05508-000, Brazil
[h] Department of Chemistry, University of Sargodha, Sargodha, Pakistan
[i] National Horizons Centre, Teesside University, Darlington, DL11HG, United Kingdom
[j] School of Health & Life Sciences, Teesside University, Middlesbrough, TS1 3BX, United Kingdom

HIGHLIGHTS

- Designing of acridine based donor materials (**HBTD2-HBTD9)** from **HBTR1** *via* efficient acceptors.
- Study of photovoltaic properties of aforesaid compounds through DFT.
- Investigation of opto-electronic properties at B3LYP/6-311G(d,p) functional of DFT.
- Efficacy of designed compounds was explored by investigating open circuit voltage.

ARTICLE INFO

Keywords:
Star-shaped
Fullerene-free donors
Triphenylamine
Charge transfer
Open circuit voltage

ABSTRACT

Fullerene-free organic chromophores have drawn considerable attention as successful photonic devices for organic solar cells. So, a series of novel non-fullerene-based donor molecules (**HBTD2–HBTD9**) were fabricated *via* structural modification of the terminal acceptor groups from **HBTR1**. In order to achieve the photovoltaic, photophysical, and electronic behavior of fore-said compounds, density functional theory/time-dependent density functional theory (DFT/TD-DFT) based analyses were accomplished at B3LYP functional along with 6-311G(d,p) basis set. The optical and electrical characteristics of the derivatives were compared with **HBTR1** architecture. All designed molecules exhibited a lower E_{HOMO}-E_{LUMO} band gap (2.183–4.106 eV) with a red shift in absorbance compared to the reference compound (4.179 eV). All derivatives (**HBTD2–HBTD9**), except **HBTD3**, showed a greater exciton dissociation rate due to low binding energy (E_b = −0.337 to 1.400 eV) when compared with **HBTR1** (E_b = 1.401 eV). Interestingly, **HBTD9** manifested to be the prime candidate for non-fullerene organic solar cells (NF–OSCs) owing to the lowest energy band gap, large mobility of charges, and least value of binding energy while holding an excellent redshift value compared to all the designed chromophores. This study revealed that these chromophores would be potential competitors in manufacturing effective optoelectronic materials.

* Corresponding author. National Horizons Centre, Teesside University, Darlington, DL11HG, United Kingdom.
** Corresponding author. Institute of Chemistry, Khwaja Fareed University of Engineering & Information Technology, Rahim Yar Khan, 64200, Pakistan.
E-mail addresses: muhammad.khalid@kfueit.edu.pk, Khalid@iq.usp.br (M. Khalid), Safwan.akram@tees.ac.uk (M.S. Akram).

https://doi.org/10.1016/j.matchemphys.2023.127528
Received 23 June 2022; Received in revised form 28 January 2023; Accepted 19 February 2023
Available online 21 February 2023

1. Introduction

The energy crisis is regarded amongst the most extensively considered issues of the world in the present era [1]. This has emerged as a consequence of a high reliance on non-renewable energy sources, which will eventually deplete, creating environmental catastrophe owing to the accumulation of greenhouse gases [2]. Solar cells, wind power, hydropower and biomass are just a few solutions that have been explored to address this issue [3]. Most promising of which are photovoltaic materials, that can transform solar power into electricity, offering a sustainable and practical solution to address the problem of rising global energy demand [4–7]. Solar cells have gained noteworthy attention, particularly in the sunny parts of the world on domestic rooftops and industrial-scale solar parks. The photoelectric effect is considered as the foundation for the working of solar cells, which transforms sunlight into electrical energy [8]. Silicon has been exploited as a semiconductor element in solar cells for decades because of its low toxicity and high thermal stability, and 46% high power conversion efficiency. On the other hand, silicon has a number of disadvantages, including hardness which limits its usage on non-tunable energy levels, high manufacturing costs and its installation on modern high-rise buildings [9,10]. Organic solar cells (OSCs) are then identified as an appropriate substitute for silicon-based solar cells because of their relatively lower manufacturing costs, lightweight, good power conversion efficiencies, tunable energy levels, and flexibility [11].

In bulk hetero-junction (BHJ), fullerene-based organic solar cells secure 11–12% power conversion efficiencies [12,13]. High electron mobility, isotropic charge transfer, and low reorganization energies are all outstanding features of fullerene derivatives ($PC_{61}BM$ and $PC_{71}BM$), making them suitable solar cell candidates than silicon-based solar cells [14,15]. Nevertheless, fullerene-based OSCs possess some limitations, including poor visible region absorption, low V_{oc}, a small number of energy levels, high band gap and high cost [16,17]. Therefore, nowadays, scientists are trying to develop non-fullerene-based organic solar cells [18] to overcome these drawbacks and improve solar cell efficiency [19]. The non-fullerene-based organic solar cells (NFA-OSCs) have improved photovoltaic features such as solubility, significant visual absorption and tunable energy levels [20,21]. Recently, non-fullerene organic solar cells (NF–OSCs) have been categorized into two classes; (i) small molecules and (ii) polymeric solar cells [22–24]. Compared to polymer, small molecule-based NF solar cells have superior optoelectronic characteristics due to their higher purity. High power conversion efficiency (PCE) has been achieved with small molecular (SM) solar cells having benzothiadiazole (BT), dithienosilole [25], and dithienopyrrole [26] core acts as electron-donating species. A triphenylamine (TPA) core is regarded as one of the most exploited electron-donating unit in producing efficient solar cell materials owing to its inexpensive cost, better electrochemical stability, and greater hole-carrying capability [27]. It's potential can be further increased by improving overall shape and positioning in the designed molecules, therefore, in this manuscript we have designed a star-shaped molecule, that have not yet been researched and characterised as a donor material in SM-OSCs for applications in organic solar cells. We hope that this star-shaped donor-based TPA core compounds may help in the creation of novel molecules for OSCs and other optoelectronic materials. Keeping in view the importance of TPA core, in the current study, a synthesized star-shaped FATPA core-based donor chromophore, *i.e.* (2,2′,2′′-((((1*E*,1′*E*,1″*E*)-((4,4,8,8,12,12-hexamethyl-8,12-dihydro-4*H*-benzo[9,1]quinolizino[3,4,5,6,7-*defg*]acridine-2,6,10-triyl)tris([2,2′-bithiophene]-5′,5-diyl))tris(thiophene,-5,2-diyl))tris(ethan-1-yl-1-yledine)trimalononitrile) named as **HBTP** is taken as a parent compound [28]. From this parent molecule, **HBTR1** and its derivatives (**HBTR2-HBTR9)** are derived to develop efficient photovoltaic materials. Various kinds of analyses, such as frontier molecular orbital analysis (FMOs), absorption spectra (UV–Vis), the density of state (DOS), transition density matrix (TDM), and open circuit voltage analysis, have been accomplished *via* density functional theory/time-dependent density functional theory. Hence, we predict that the entitled candidates might possess significant photovoltaic responses and be used as efficient solar cell devices.

2. Computational procedure

For the execution of all analyses, Gaussian 09 package [29] was utilized, and all the inputs of **HBTR1** and **HBTD2-HBTD9** were drawn with GaussView 6.0 [30]. First, **HBTP,** which was taken as parent compounds, was optimized at different levels of theory, such as B3LYP [31], CAM-B3LYP [32], MPW1PW91 [33], M06 [34], and M06–2X [35] in conjugation with 6-311G(d,p) as a basis set. After successfully optimizing **HBTP** at all selected functionals, UV–Vis analysis was performed at all the functionals of DFT. A comparative analysis was made between experimental and simulation values of λ_{max} to select the suitable functional for the DFT study. The simulated λ_{max}values in tetrahydrofuran were obtained as 627.58 (M06), 472.374 (M06–2X), 539.671 (B3LYP), 464.238 (CAM-B3LYP), and 541.108 (MPW1PW91) *nm*. Among all functionals, B3LYP [16,36–38] with 6-311G(d,p) [39] showed good harmony with the experimental result (508 nm), as shown in Fig. 1. After selecting the B3LYP level, **HBTR1** and **HBTD2-HBTD9** chromophores were optimized at the selected level for further study.

Furthermore, for investigating the optoelectronic properties and the structure-property relationship of entitled molecules, frontier molecular orbitals (FMOs), the density of states (DOS), transition density matrix (TDM), absorption spectra (UV–Vis), open-circuit voltage (V_{oc}) analyses were accomplished at B3LYP level and 6-311G(d,p) basis set. The software, PyMOlyze [40], Multiwfn 3.7[41], GaussSum [42], Avogadro [43] and Chemcraft [44] were utilized for the analysis of all data.

3. Results and discussion

In the current study, a synthesized star-shaped donor chromophore, **FATPA** [28], was used to develop **HBTP** (Parent chromophore) by replacing the larger bulky alkyl group ($-C_5H_{11}$) in fused triphenylamine with a smaller alkyl unit ($-CH_3$), in order to reduce the computational cost and time (see Fig. 2). From this parent chromophore, another chromophore, **HBTR1**, was designed and utilized as a reference molecule in the current study. **HBTR1** consists of 4,4,8,8,12,12-hexamethyl-3a1,4,4a1,7a,8,8a1,11a,12-octahydro-3aH-benzo[1,9]quinolizino

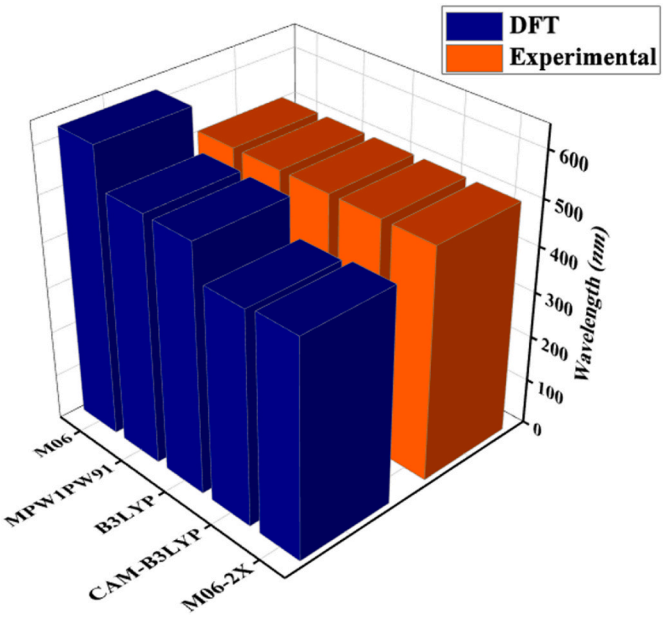

Fig. 1. Comparison of maximum absorption values of **HBTP** between experimental and DFT at various levels of theory.

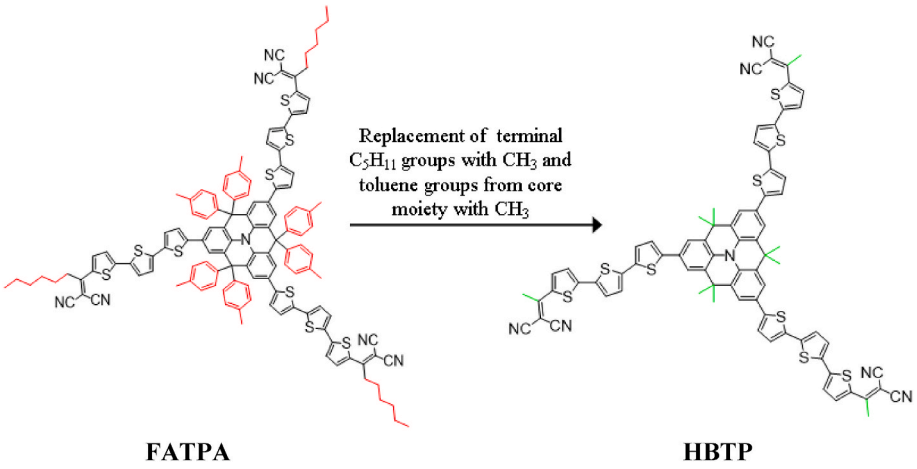

Fig. 2. Modification of **FATPA** into **HBTP** *via* substitution of methyl (-CH_3) group.

[3,4,5,6,7-defg]acridine-based donor core unit which is an acridine-based fused derivative of triphenylamine, making the center of the star. Thiophene rings act as π-spacers, and hexyldicyanovinyl acts as a terminal acceptor unit; both π-spacers and acceptor form the arms of the star. From the literature, we found that the photovoltaic properties of molecules could be enhanced by structural tailoring with various efficient acceptors [45]. Therefore, structural modeling of **HBTR1** has been performed with various efficient acceptor moieties (see Fig. S2), and a series of acridine-based chromophores **HBTD2–HBTD9** is designed. (Scheme 1 and Fig. S1). The optimized geometries of the above-mentioned compounds are shown in Fig. 3, and their cartesian coordinates are tabulated in Tables S1–S9. After the structural modification, a DFT study was performed at B3LYP/6-311G(d,p) functional to examine the photovoltaic properties.

4. Frontier molecular orbital (FMO) analysis

In an organic system, electronic and optical characteristics of the compounds can easily be found *via* FMO study. It is a prime tool for understanding optoelectronic properties [46–48]. The HOMO/LUMO characterization is auspiciously achieved through band theory, which perceives LUMO as a conduction band, whereas HOMO is a valence band [49–52]. The flow of electronic clouds between the molecular orbitals (MO) can be understood by the charge distribution pattern on the HOMO and LUMO orbitals [53,54]. So, FMO's energy band gap (E_{gap} = E_{HOMO}-E_{LUMO}) is regarded as an excellent parameter [55–58] which gives understanding regarding the charge transference in photovoltaic molecules. Literature supported that the probability of electronic charge transport can be improved in the organic systems *via* incorporating electron-withdrawing groups that facilitate the delocalization of electronic cloud in the molecular systems. Hence, FMO analysis is employed for the designed donor **HBTR1**, and **HBTD2-HBTD9** molecules and their findings are tabulated in Table 1.

The calculated energy of HOMO and LUMO was observed to be −6.499 and −2.320 eV, with a 4.179 eV energy gap for **HBTR1**. The energy gap was examined to be decreased in all the designed chromophores due to the modeling of acceptor unit with different electronegative substituents. E_{HOMO} were noted to be −5.518, −6.516, −6545, −5.518, −6.638, −5.173, −5.439 and −5.469 eV and E_{LUMO} were found to be −3.107, −2.410, −2.473, −3.210, −3.072, −2.611, −3.064 and −3.286 eV for **HBTD2-HBTD9**, respectively. The band gap is believed to be the most important characteristic to illustrate the transferability of electron density and optoelectronic characteristics in compounds [59]. The ΔE values of designed chromophores (**HBTD2-HBTD9**) were determined to be 2.501, 4.106, 4.072, 2.308, 3.566, 2.562, 2.375 and 2.183 eV, respectively. The compound **HBTD3** possessing

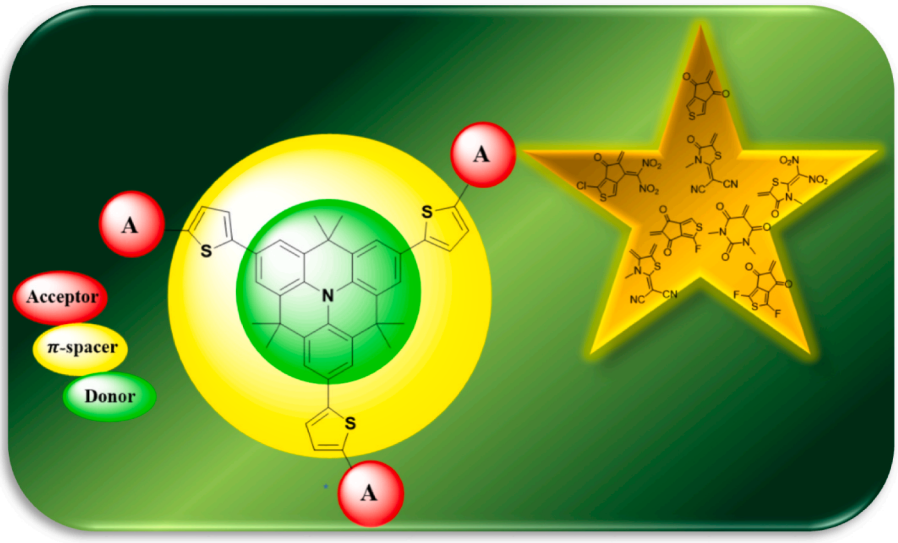

Scheme 1. The sketch map of the reference (**HBTR1**) and derivatives (**HBTR2-HBTR9**).

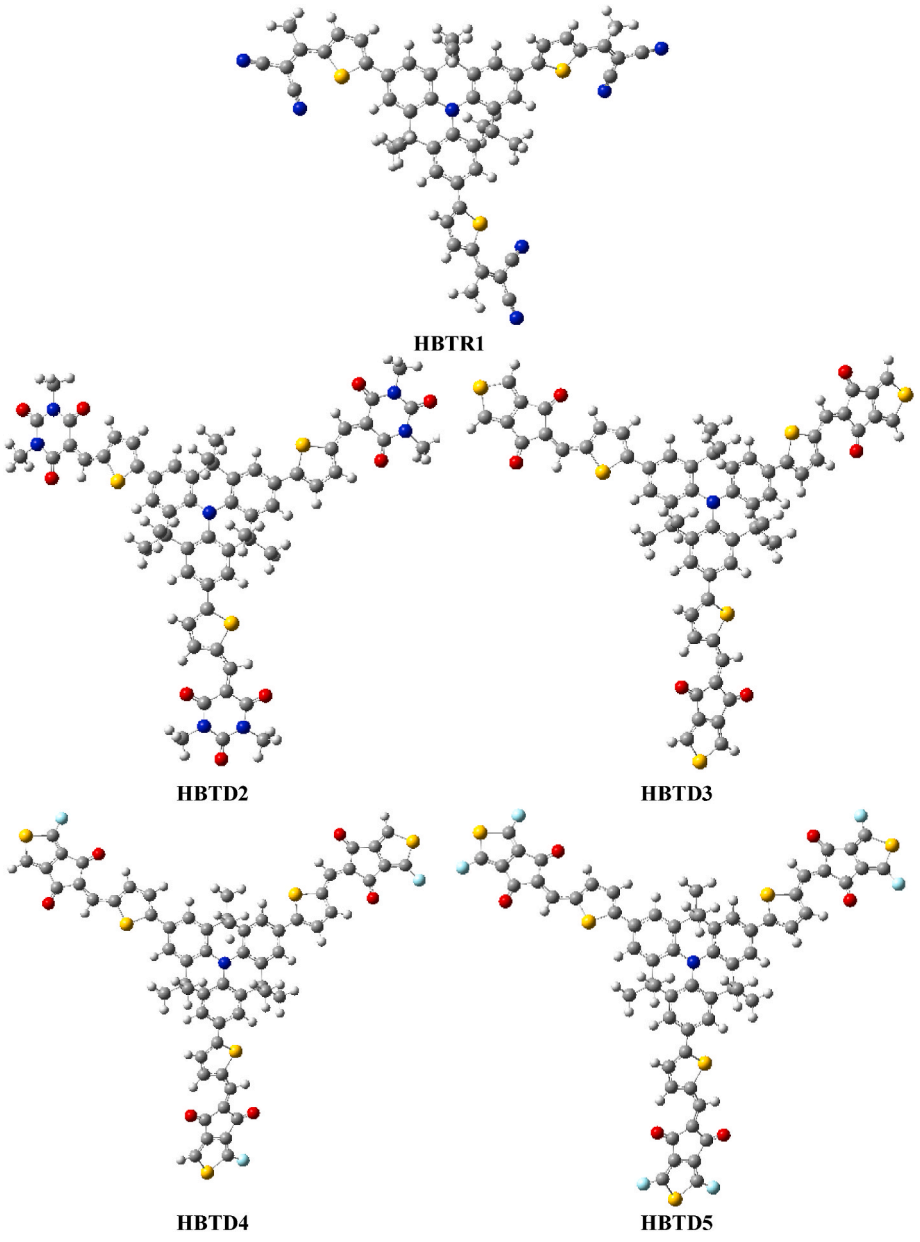

Fig. 3. Optimized structures of **HBTR1** and **HBTD2-HBTD9** with the natural atomic coloring scheme.

5-ethylidene-4*H*-cyclopenta[*c*]thiophene-4,6(5*H*)-dione as the end-capped acceptor exhibited a slightly lower value of E_{gap} (4.106 eV) in comparison with the reference molecule *i.e.,* **HBTR1 (**4.179 eV) due to improved resonance. and –*I* effect of C=O groups at terminal acceptor region. Similarly, lowering in the band gap is seen in **HBTD4** (4.072 eV) owing to the presence of a strongly electronegative fluoro (–F) functional group at the peripheral acceptor moiety ((Z)-5-ethylidene-1-fluoro-4*H*-cyclopenta[*c*]thiophene-4,6(5*H*)-dione). Further, a decrease in band gap (3.566 eV) is observed for **HBTD6** in which the terminal acceptor unit is ((*Z*)-3-chloro-6-(dinitromethylene)-5-ethylidene-5,6-dihydro-4*H*-cyclopenta[*c*]thiophen-4-one) containing chloro (–Cl) and nitro (–NO_2) groups possessing enhanced resonance and strong electron-withdrawing nature, respectively. In **HBTD7**, the E_{HOMO}-E_{LUMO} gap again reduced to 2.562 eV by introducing an acceptor moiety as ((*E*)-2-(5-ethylidene-3-methyl-4-methylenethiazolidin-2-ylidene)malononitrile) containing cyano (–CN) groups. The higher negative inductive (-*I*) effect of –CN, as compared –Cl, may be a cause of this band gap reduction. This E_{gap} is found to be reduced to 2.501 eV, expressed by **HBTD2** containing three carbonyl groups on the acceptor arm (5-ethylidene-1,3-dimethylpyrimidine-2,4,6-(1*H*,3*H*,5*H*)-trione). This reduced E_{gap} might be due to further enhancement in the resonance and electron-withdrawing effect over the acceptor region. Interestingly, in **HBTD8**, sp^2 hybridized sulphur (-S) is present in the acceptor region; ((*E*)-2-(5-ethylidene-3-methyl-4-oxothiazolidin-2-ylidene)malononitrile), which is largely efficient to improve the resonance [60] and lessen the energy band gap between HOMO/LUMO, which further decreased E_{gap} to 2.375 eV. Further, a decline in HOMO/LUMO energy difference (2.308 eV) is observed in **HBTD5** because of the existence of two –F groups with greater negative inductive (–*I*) effect on the acceptor (5-ethylidene-1,3-difluoro-4*H*-cyclopenta[*c*]thiophene-4,6(5*H*)-dione). The smallest band gap (2.183 eV) is found to be observed in the case of **HBTD9** in which two strong electron-withdrawing nitro (–NO_2) groups on the acceptor moiety as ((*E*)-2-(dinitromethylene)-5-ethylidene-3-methylthiazolidin-4-one). The decrease in energy gap is owing to the

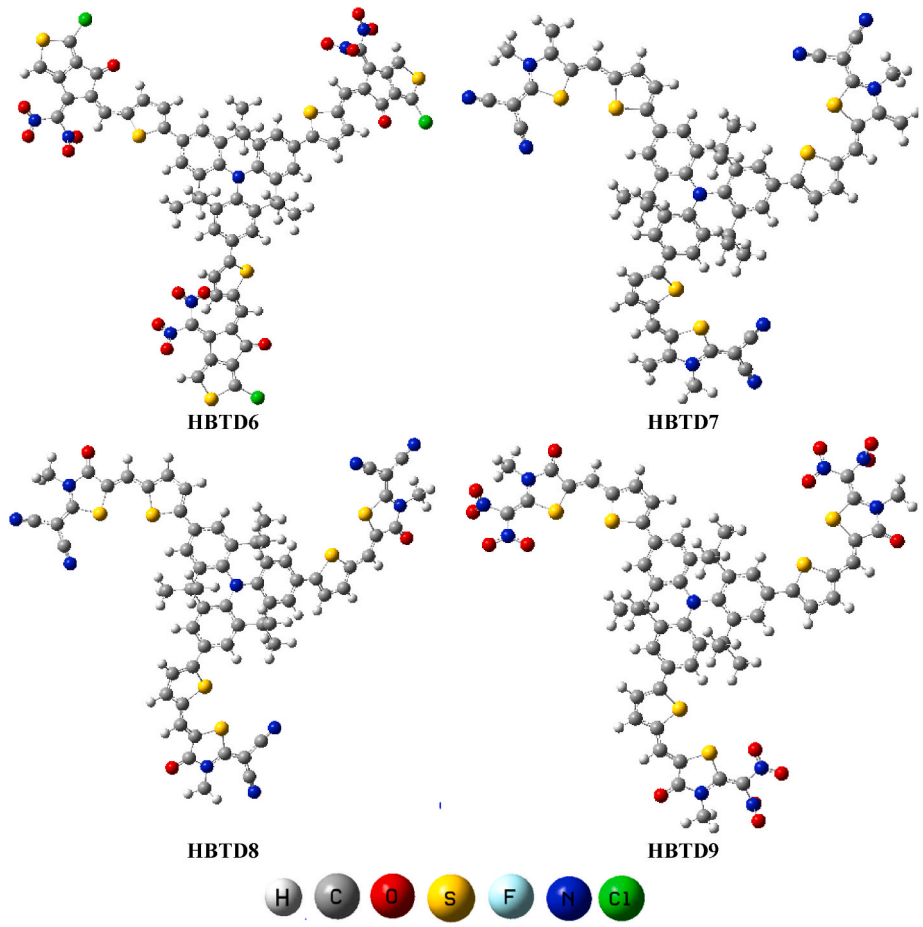

Fig. 3. (*continued*).

Table 1
E_{HOMO}, E_{LUMO} and energy gap (E_{LUMO}-E_{HOMO}) of **HBTR1** and **HBTD2-HBTD9**.

Compounds	E_{HOMO}	E_{LUMO}	Band Gaps
HBTR1	−6.499	−2.320	4.179
HBTD2	−5.518	−3.017	2.501
HBTD3	−6.516	−2.410	4.106
HBTD4	−6.545	−2.473	4.072
HBTD5	−5.518	−3.210	2.308
HBTD6	−6.638	−3.072	3.566
HBTD7	−5.173	−2.611	2.562
HBTD8	−5.439	−3.064	2.375
HBTD9	−5.469	−3.286	2.183

Units in *eV*.

improved –*I* effect of $–NO_2$ compared to the –CN (NO_2>CN) [61]. Overall, the descending trend of energy gaps of **HBTR1** and **HBTD2-HBTD9** is in the following order: **HBTR1** > **HBTD3** > **HBTD4** > **HBTD6** > **HBTD7** > **HBTD2** > **HBTD8** > **HBTD5** > **HBTD9**. Additionally, the surfaces of FMOs have also been used to demonstrate electronic density transfer phenomena [62], as shown in Fig. 4. In all investigated compounds, the large amount of electronic cloud for HOMO is concentrated over the donor (4,4,8,8,12,12-Hexamethyl-4*H*,8*H*,12*H*.12*c*-aza-dibenzo[*cd*,*mn*]pyrene) and π-bridge (thiophene) while LUMO is positioned mainly over the end-capped acceptor units. It is now convinced from the aforementioned study that all the derivatives have lower energy band gaps (Table 1) between HOMO/LUMO; hence, the entitled compounds might prove to be promising candidates with efficient optoelectronic properties.

5. Absorption analysis

To further estimate the performance of OSCs, UV–Vis spectral analysis [55] of **HBTR1** and **HBTD2**–**HBTD9** was executed with TD-DFT at B3LYP functional and 6-311G (d,p) basis set conjugation in the organic solvent (tetrahydrofuran) and gas phase [63]. UV–Vis analysis offers useful computational aspects for understanding the electronic excitations, contributing configurations and rate of charge shifting phenomenon within the studied molecules [56]. During TD/DFT computations [64], obtained absorption spectra of **HBTR1** and **HBTD2**–**HBTD9** are depicted in Fig. 5. Various computationally calculated parameters like maximum absorption wavelength (λ_{max}), transition energy (E^{DFT}) and molecular orbital contributions, and the results for **HBTR1** and **HBTD2**–**HBTD9** in gaseous phase and solvent are outfitted in Table 2. Other prominent molecular orbital contributions and details are provided in Tables S10–28.

Results indicate that absorbance exhibited by all the investigated chromophores fell in the visible range. It is evident from Table 2 that electronic transitions of all the designed chromophores took place at higher wavelengths than the reference compound (**HBTR1** as 446.243 nm) except **HBTD7** (429.933 nm) in the solvent. But in the gaseous state, all the designed derivatives (**HBTD2-HBTD9**) displayed a red shift in absorption spectra compared with **HBTR1**. However, absorption maxima are largely influenced by the change in bond polarity and the solvent's nature, which can be conveniently seen *via* a prominent bathochromic shift in D-A configured compounds in the solvent phase [65]. The absorption maximum for **HBTD9** (659.175 nm) is observed to be the highest, with an oscillator strength of 0.750 and the lowest excitation energy of 1.881 eV. This implies that **HBTD9** shows the highest red shift in the solvent compared with other molecules of this

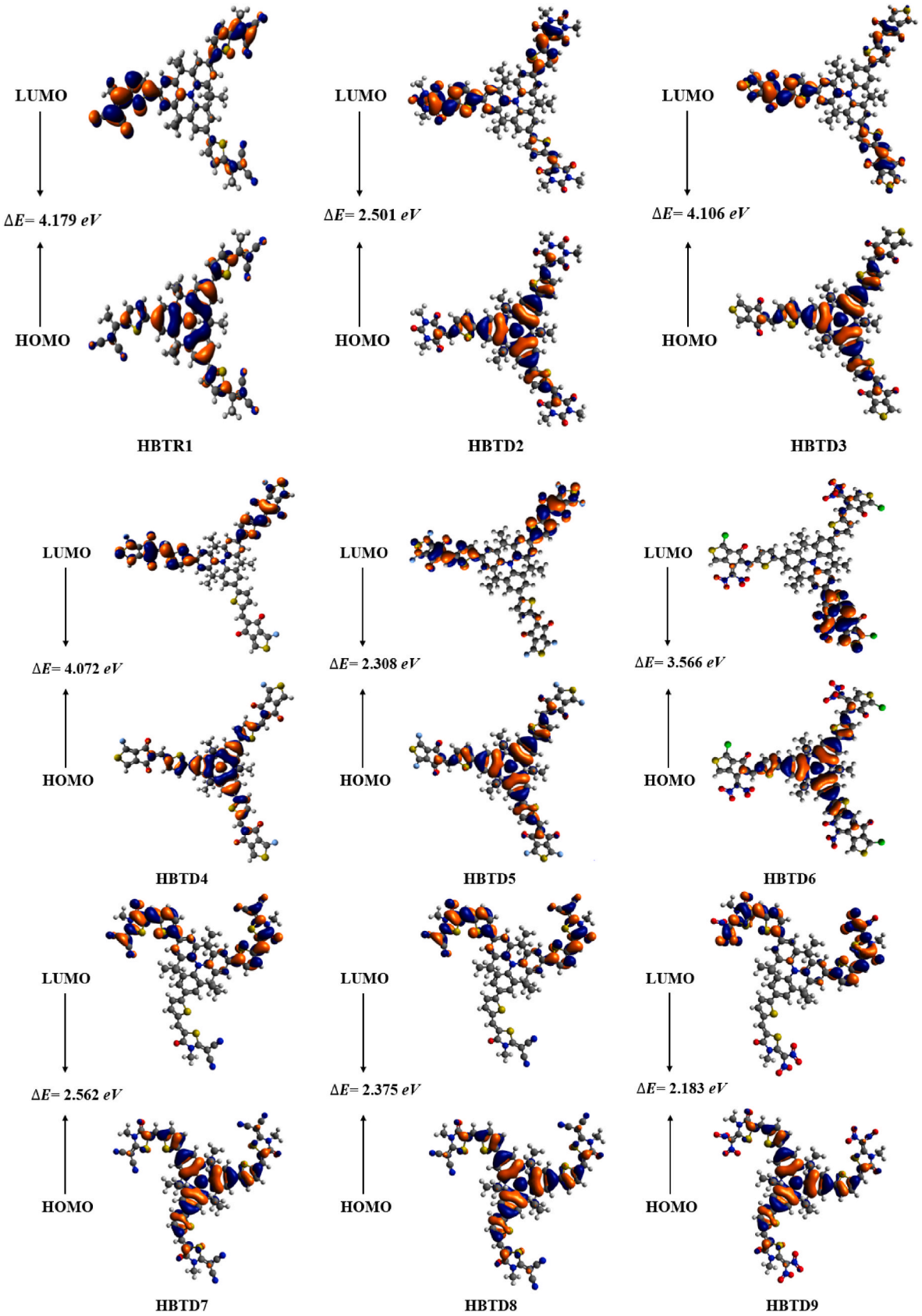

Fig. 4. Pictorial depiction of density distribution pattern in HOMO/LUMO of **HBTR1** and **HBTD2-HBTD9**.

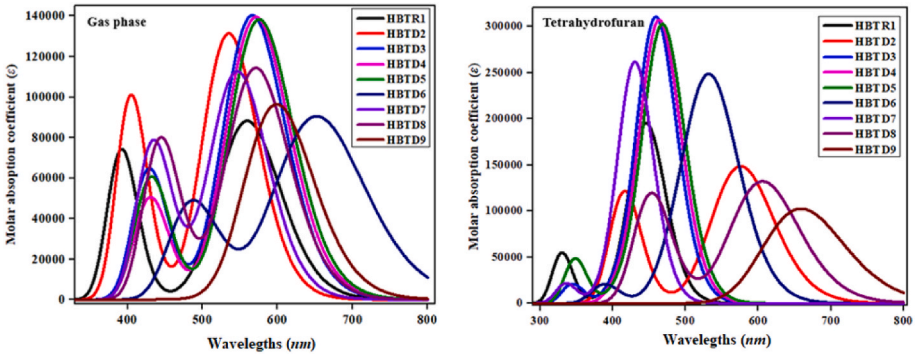

Fig. 5. Absorption spectra of **HBTR1** and **HBTD2–HBTD9**.

Table 2
Calculated maximum absorption wavelengths (λ_{max}), transition energy (eV), molecular orbital contributions, and oscillator strengths (f_{os}) of compounds **HBTR1** and **HBTD2–HBTD9**.

	Compounds	λ (*nm*)	*E* (*eV*)	f_{os}	MO contributions
A[a]	**HBTR1**	392.367	3.160	0.683	H-2→L (52%), H-1→L+1 (44%),
	HBTD2	534.807	2.318	0.921	H→L+1 (99%)
	HBTD3	566.267	2.190	0.976	H→L+1 (99%)
	HBTD4	571.356	2.170	0.948	H→L+1 (91%), H→L (8%)
	HBTD5	575.600	2.154	0.960	H→L+1 (97%), H→L (2%)
	HBTD6	644.945	1.922	0.731	H→L+1 (97%)
	HBTD7	544.985	2.275	0.817	H→L+1 (97%)
	HBTD8	569.806	2.176	0.833	H→L+1 (97%)
	HBTD9	597.860	2.074	0.698	H→L+1 (96%), H→L (3%)
B[b]	**HBTR1**	446.243	2.778	1.710	H→L (74%), H-2→L (5%)
	HBTD2	575.680	2.154	1.040	H→L+1 (99%)
	HBTD3	459.439	2.699	2.140	H→L+1 (66%), H-2→L (6%)
	HBTD4	463.995	2.672	2.094	H→L+1 (67%), H-2→L+1 (6%)
	HBTD5	468.714	2.645	2.068	H-2→L+2 (11%), H→L+1 (68%)
	HBTD6	528.965	2.344	1.910	H-1→L+2 (15%), H→L+1 (66%)
	HBTD7	429.933	2.884	1.879	H-2→L+2 (11%), H→L+1 (60%)
	HBTD8	605.569	2.047	0.966	H→L+1 (96%)
	HBTD9	659.175	1.881	0.750	H→L+1 (92%), H→L (7%)

A[a] = gas phase, B[b] = tetrahydrofuran.

series, which can be attributed to the strong electron-withdrawing nature of -nitro groups. So, it is clear that absorption maxima (λ_{max}) can be efficiently enhanced by the introduction of electron-withdrawing groups [66]. However, under gas-phase conditions, the strongest redshift effect is found for **HBTD6**. On the contrary, the least absorbance value is obtained for **HBTD7** at 429.933 nm with the highest transition energy of 2.884 eV in tetrahydrofuran. The absorption wavelength of **HBTD2–HBTD9** was calculated to be 575.680, 459.439, 463.995, 468.714, 528.965, 429.933, 605.569, and 659.175 nm, respectively. The decreasing order of maximum absorbed wavelength of entitled molecules is **HBTD9** > **HBTD8** > **HBTD2** > **HBTD6** > **HBTD5** > **HBTD4** > **HBTD3** > **HBTR1** > **HBTD7**. On the contrary, the excitation energies of studied dyes decrease in the following manner **HBTD7** > **HBTR1** > **HBTD3** > **HBTD4** > **HBTD5** > **HBTD6** > **HBTD2** > **HBTD8** > **HBTD9**. As evident from the literature, there is a high probability of charge transference in bathochromically shifted molecules possessing low excitation energy.

6. Transition density matrix (TDM) analysis

Transition density matrix analysis (TDM) reveals the transition and movement of an electronic cloud in an organic system. TDM plots offer a better understanding of the location of excited electrons, holes and electrons within organic solar cells (OSCs), providing a 3-D display of electron-hole pair distribution and delocalization [48]. The TDM heat maps are the most convenient way to locate the enhanced exciton dissociation in their excited states, which is crucial in developing solar cells [67]. The calculations are achieved at B3LYP level of theory and 6-311G(d,p) basis set. Due to the least contributions of hydrogen atoms, they are neglected in this analysis. All the designed derivatives are regarded as A-π-D-π-A structures having three major portions (i) Donor, (ii) π-spacer and (iii) Acceptor. Therefore, the charge transfer is determined diagonally from the donor towards the acceptor region *via* π-spacer, as shown in Fig. 6.

The transition density maps show a good electronic charge coherence in **HBTD3**, **HBTD4**, **HBTD5** and **HBTD6** compounds where a prominent diagonal shift can be seen. Overall, the results have revealed that the excitations are much confined to the donor and π-bridge portion.

The exciton binding energy (E_b) is a crucial factor in determining the rate of charge separation and is directly related to the columbic force between the hole and electron [68]. The lower E_b values indicate weaker electron-hole interactions, thus increasing the charge transfer process [69]. Equation (3) represents the relationship among binding energy, energy band gap and energy of optimization [70].

$$E_b = E_{H\text{-}L} - E_{opt} \quad \text{Eq (3)}$$

The results obtained from Equation (3) are recorded in Table 3. The maximum value of E_b is displayed by **HBTD3** as 1.407 eV, and the compound **HBTD5** showed the least value (−0.337 eV). The exciton binding energy in the entitled compounds decreases in the following order: HBTD3 > HBTR1 > HBTD4 > HBTD6 > HBTD2 > HBTD8 > HBTD9 > HBTD7 > **HBTD5**. Interestingly, all the studied chromophores have shown E_b values less than 1.9 eV, which indicates a higher exciton dissociation rate with a larger rate of charge transfer and could be considered good materials for NF–OSCs [71].

7. Density of states (DOS) analysis

DOS investigation is accomplished to define the electronic states contribution that holds electrons at a particular energy state of the overall molecular system. A zero value of DOS indicates the unavailability of energy states to be occupied at a given energy band. The density of states calculations provide a wide range of energy states to be evaluated and help estimate the E_{gap} [72]. Hence, DOS analysis aids in the demonstration of the results explained in FMOs and the percentage charge densities of HOMOs and LUMOs. This study was accomplished at the B3LYP level and 6-31G (d,p) basis set conjugation. In the current study, to compute DOS, **HBTR1** and **HBTD2-HBTD9** are separated into three sections, *i.e.*, donor (D), π-linker and end-capped acceptor (A) groups. In DOS pictographs, the distribution pattern of the D, π-spacer and A moieties are displayed by red, green and blue colored lines,

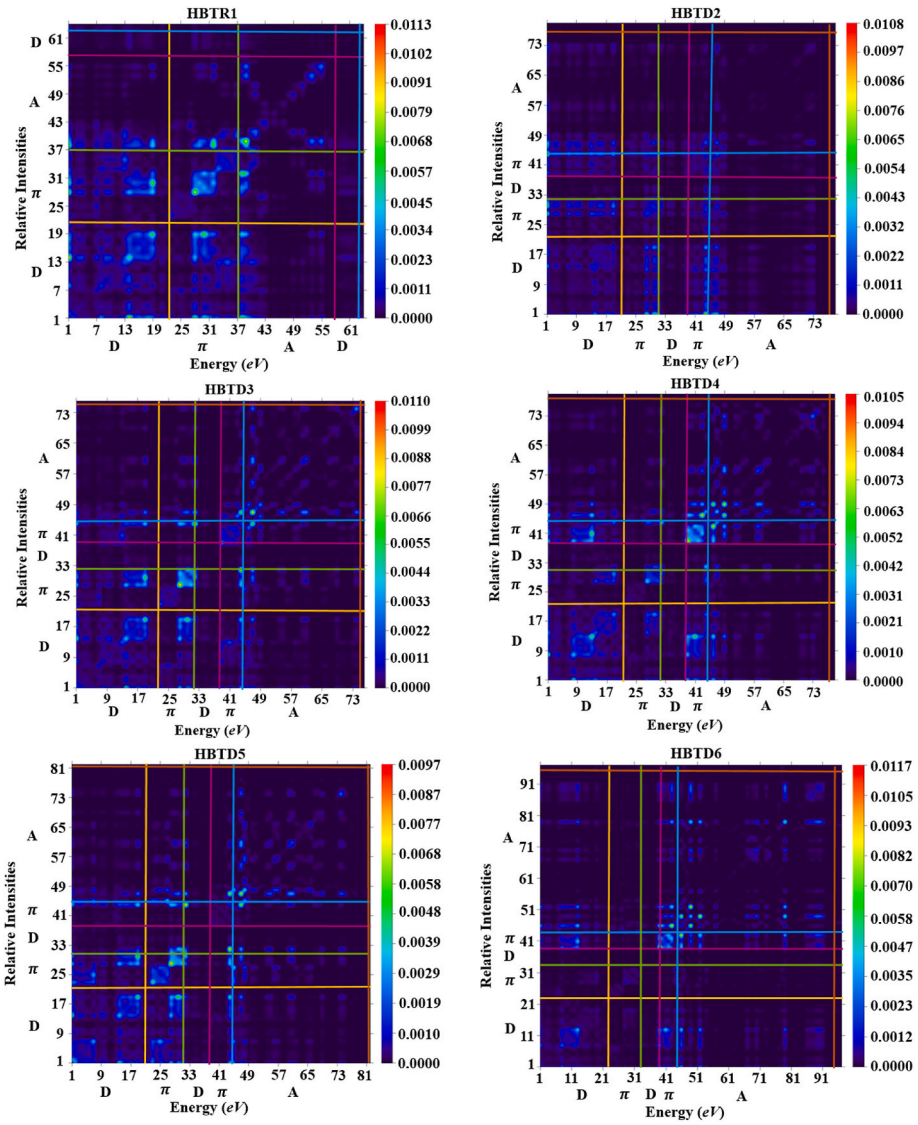

Fig. 6. TDM heat maps of reference (**HBTR1**) and designed derivatives (**HBTD2**-**HBTD9**).

respectively (Fig. 7). The valence band (HOMO) is shown by the negative values, positive values denote the conduction band (LUMO) along the x-axis, and the interval between the valence and conduction band is designated as a band gap [41,73]. For **HBTR1,** the donor donates 12.0% to LUMO and 74.3% to HOMO, while the π-linker supplies 36.5% to LUMO and 17.0% to HOMO. Similarly, the contribution of the acceptor to LUMO is 51.5% and to HOMO is 8.6% in **HBTR1**. The donor contributes 12.6, 9.9, 9.8, 10.3, 4.7, 11.3, 10.1 and 6.4% to LUMO and 68.8, 66.7, 67.1, 68.4, 66.7, 55.6, 62.9 and 63.7% to HOMO in **HBTD2-HBTD9**, respectively. In the same way, π-spacer provides 34.6, 28.5, 28.6, 28.2, 15.8, 26.8, 27.8 and 19.3% to LUMO, whereas 19.7, 20.5, 20.1, 18.9, 18.5, 24.6, 21.2 and 20.8% to HOMO for **HBTD2-HBTD9**, accordingly. Similarly, for **HBTD2-HBTD9** acceptor contributes 52.8, 61.6, 61.7, 61.6, 79.5, 61.9, 62.1 and 74.4% to LUMO, while 11.6, 12.8, 12.8, 12.8, 14.8, 19.8, 15.9 and 15.5% to HOMO, respectively. DOS reflects that numerous electron-withdrawing groups are responsible for various electronic charge distribution patterns. Furthermore, electronic transitions are also accountable for intermolecular charge transfer (ICT). Fig. 6 discloses that the uppermost peak for electronic charge distribution for HOMO is examined at the D portion from −1 to −3 eV, whereas in LUMO, it emerges in acceptor units at 1.5–3 eV in all the investigated systems. Thus, these energy ranges are remarkable and manifest that D and peripheral A moiety along with π-bridge are principally accountable for originating HOMO and LUMO in all derivatives and reinforced the FMOs analysis.

8. Open circuit voltage

The open-circuit voltage (V_{oc}) examination is utilized to estimate the operational mechanism and execution of OSCs [5,74]. It measures the total amount of electric current drawn from an optical device [75]. V_{oc} is studied at zero voltage in solar equipment. Two important parameters, *i.e.*, saturation voltage and photo-generated current, are crucial to determine the open-circuit voltage of a solar cell device. Both of these currents are important in the reintegration of solar equipment [76].

Certain measuring factors have been established for V_{oc} measurement purposes, which can be used for precise estimation of V_{oc} of a solar cell. The scaling of HOMO of donor material is done with LUMO of acceptor material [75]. The donor materials' LUMO energy must be greater than the acceptor materials' LUMO energy for larger open circuit voltage levels and efficient transfer of charge from donor to acceptor material [77]. Because all of the reference and designed molecules in

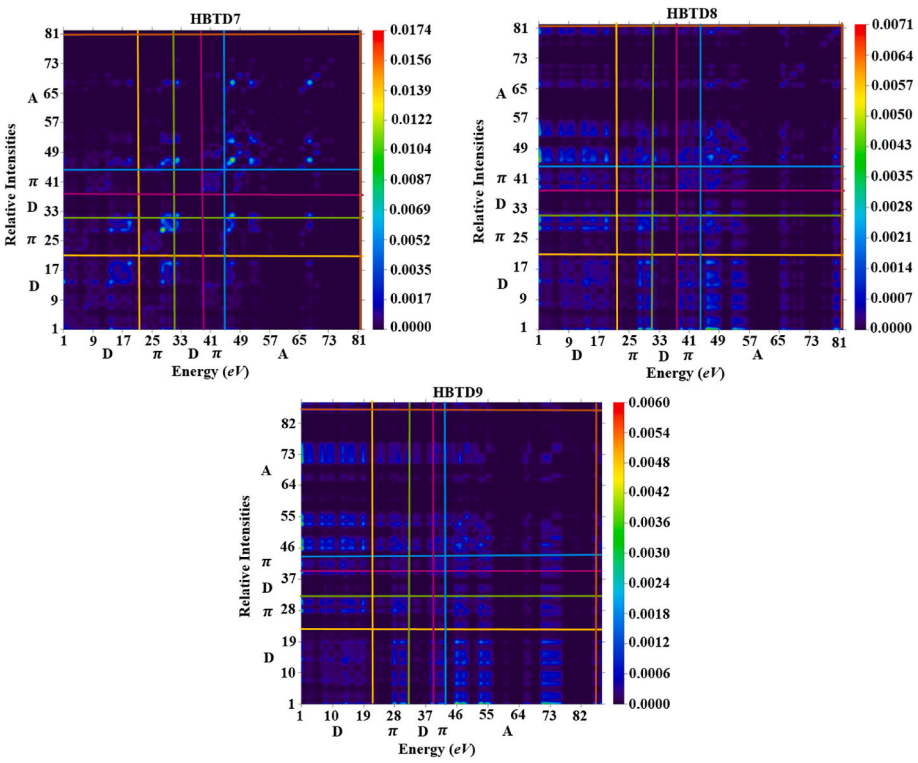

Fig. 6. (*continued*).

Table 3
E_{opt}, energy gap = $E_{H\text{-}L}$, and (E_b) of investigated compounds.

Compounds	$E_{H\text{-}L}(eV)$	$E_{opt}(eV)$	E_b (eV)
HBTR1	4.179	2.778	1.401
HBTD2	2.501	2.154	0.347
HBTD3	4.106	2.699	1.407
HBTD4	4.072	2.672	1.400
HBTD5	2.308	2.645	−0.337
HBTD6	3.566	2.344	1.222
HBTD7	2.562	2.884	−0.322
HBTD8	2.375	2.047	0.328
HBTD9	2.183	1.881	0.302

this study are donor molecules, we used the **$PC_{71}BM$**, fullerene acceptor molecule, for open circuit voltage measurements. **$PC_{71}BM$** is a well-known and widely utilized acceptor material for solar cell applications [78]. The V_{oc} calculation [79] of molecules can be accomplished using Equation (4):

$$V_{oc} = \left(\left|E^{D}_{HOMO}\right| - \left|E^{A}_{LUMO}\right|\right) - 0.3 \qquad \text{Eq (4)}$$

Where E denotes energy and the constant, *i.e.* 0.3, has been derived from the resolution of voltage drop factors [80]. One of the major goals of V_{oc} is to align the HOMO of donor-designed molecules, such as HBTR1, to the LUMO of a well-known acceptor, $PC_{71}BM$. The findings are presented in Table 4, and the pictorial representation is displayed in Fig. 8.

The above data reveals that all derivatives exhibit V_{oc} values in the range of 1.708–2.907 *V*. The ΔE among the HOMO/LUMO of donor/acceptor complexes, respectively, has been observed to be 3.068, 2.087, 3.085, 3.114, 2.087, 3.207, 1.742, 2.008 and 2.038 eV, for **HBTR1** and **HBTD2-HBTD9**, respectively (Table 4). The V_{oc} of **HBTR1** with respect to $HOMO_{HBTR1}$ −$LUMO_{PC71BM}$ is 2.768 *V*, while **HBTD6** has the greatest voltage value (V_{oc} = 2.907 *V*) among all the drafted compounds, which could be owing to efficient electron-withdrawing moieties with ideal planar geometry that permitted the maximal transfer of electronic charge from donor to acceptor region. The descending order of V_{OC} values of investigated compounds is **HBTD6** > **HBTD4** > **HBTD3** > **HBTR1** > **HBTD2** = **HBTD5** > **HBTD9** > **HBTD8** > **HBTD7**. These chromophores have been proven to be good candidates for NF–OSCs as they produce a substantial amount of voltage.

9. Molecular electrostatic potential

Molecular electrostatic potential (MEP) is a three-dimensional (3D) system of atoms to display the electronic charge density spread over various electronegative atoms. The electronic concentration over the external surface of the system is represented as a dynamic MEP design, which can anticipate the reactive nature and plausible active sites for the nucleophilic and electrophilic attack through coloration [81,82]. The declining order of electronic charge participation and electrostatic potential (EP) is: blue > green > yellow > orange > red [83]. In Fig. 9, red colors characterizes the highly electronegative oxygen (O) atom, which is susceptible to nucleophilic attack. Whereas yellow and green colors display sulphur (S) and chlorine (Cl) atoms, respectively, with less electronegative and are more susceptible to electrophilic attack due to the high electronic charge density of O, Cl and S atoms. Furthermore, the blue color specifies the nitrogen (N) atom with a negative potential. However, the grey color characterizes the electropositive carbon (C) and hydrogen (H) atoms showing the favorable sites for nucleophilic attack. Summarizing the aforementioned results, it can be concluded that electrophilic species attack the yellow and red-shaded areas on the MEP surface, while nucleophilic species attack the blue-shaded regions over the MEP surface [84].

10. Conclusion

In the current study, quantum chemical computations were accomplished to examine the photovoltaic, photophysical and electronic features of **HBTR1** and **HBTD2-HBTD9**. Eight new star-shaped molecules (**HBTD2-HBTD9**) were designed *via* a structural tailoring approach in the **HBTR1** molecule. All designed compounds have shown appealing consequences for various computational calculations. The least value of

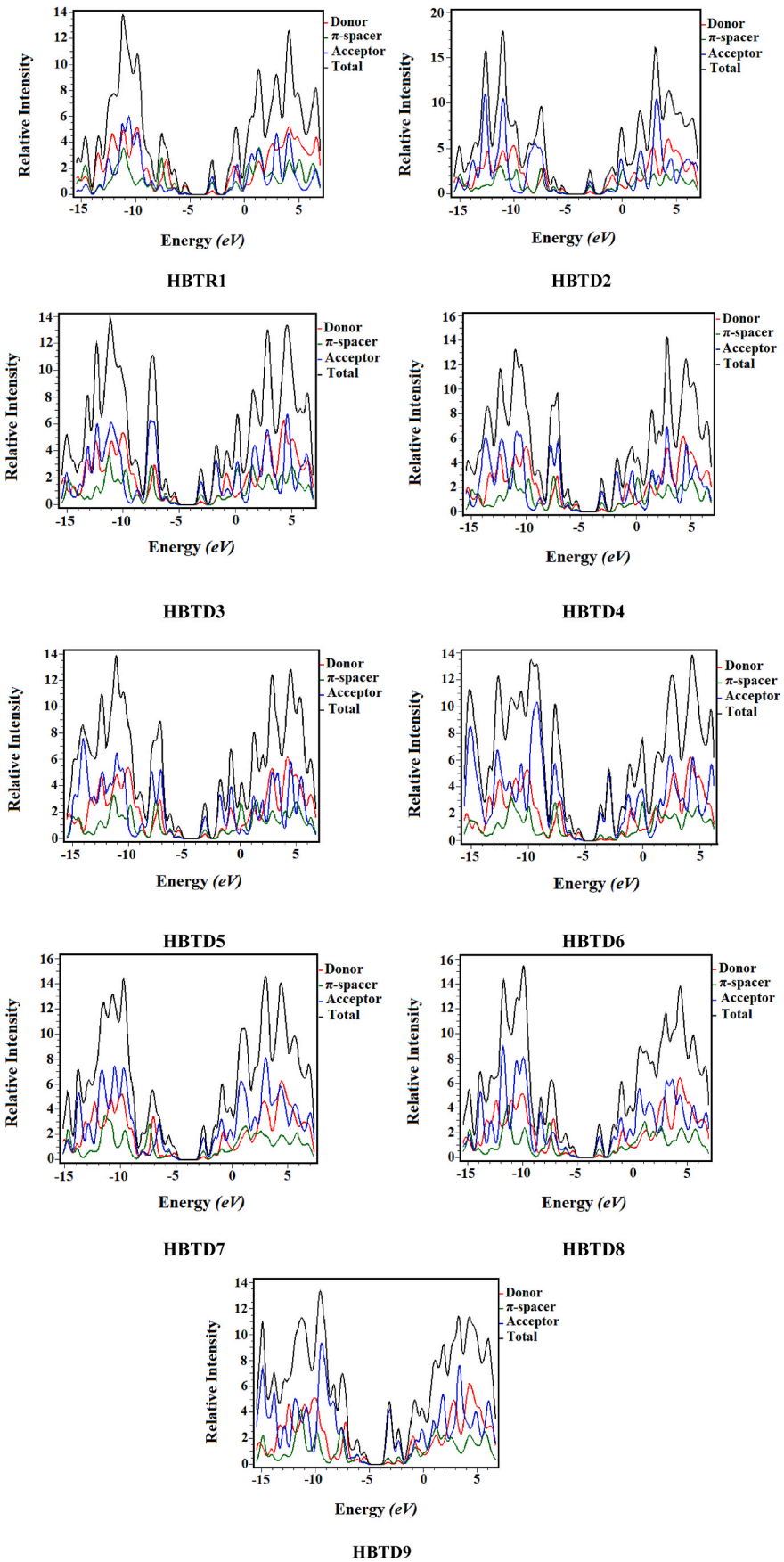

Fig. 7. Graphical illustration of DOS for **HBTR1** and **HBTD2**-**HBTD9**.

Table 4
Calculated V_{oc} results and energy band gap values of HBTR1 and HBTD2-HBTD9.

Comp.	HBTR1	HBTD2	HBTD3	HBTD4	HBTD5	HBTD6	HBTD7	HBTD8	HBTD9
V_{oc}	2.768	1.787	2.785	2.814	1.787	2.907	1.442	1.708	1.738
ΔE	3.068	2.087	3.085	3.114	2.087	3.207	1.742	2.008	2.038

ΔE = band gap between the orbitals (HOMO/LUMO) of donor/acceptor complexes.

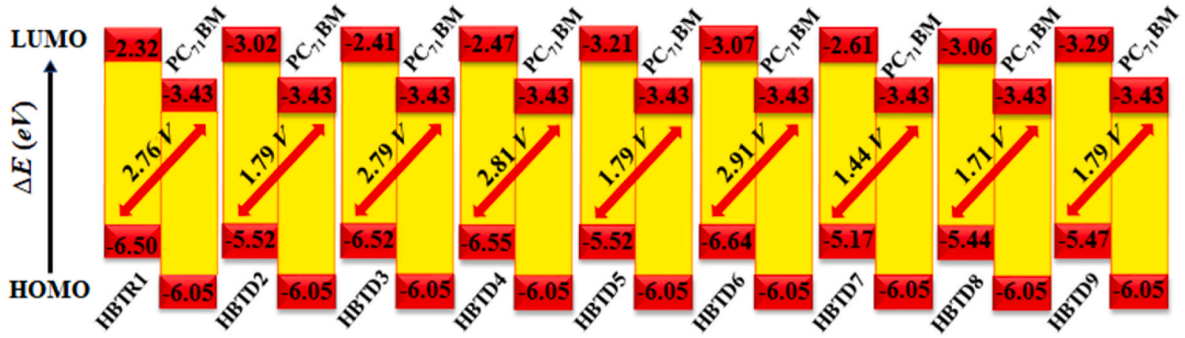

Fig. 8. Graphical representation of *Voc* for entitled chromophores (**HBTR1** and **HBTD2-HBTD9**) with **$PC_{71}BM$**.

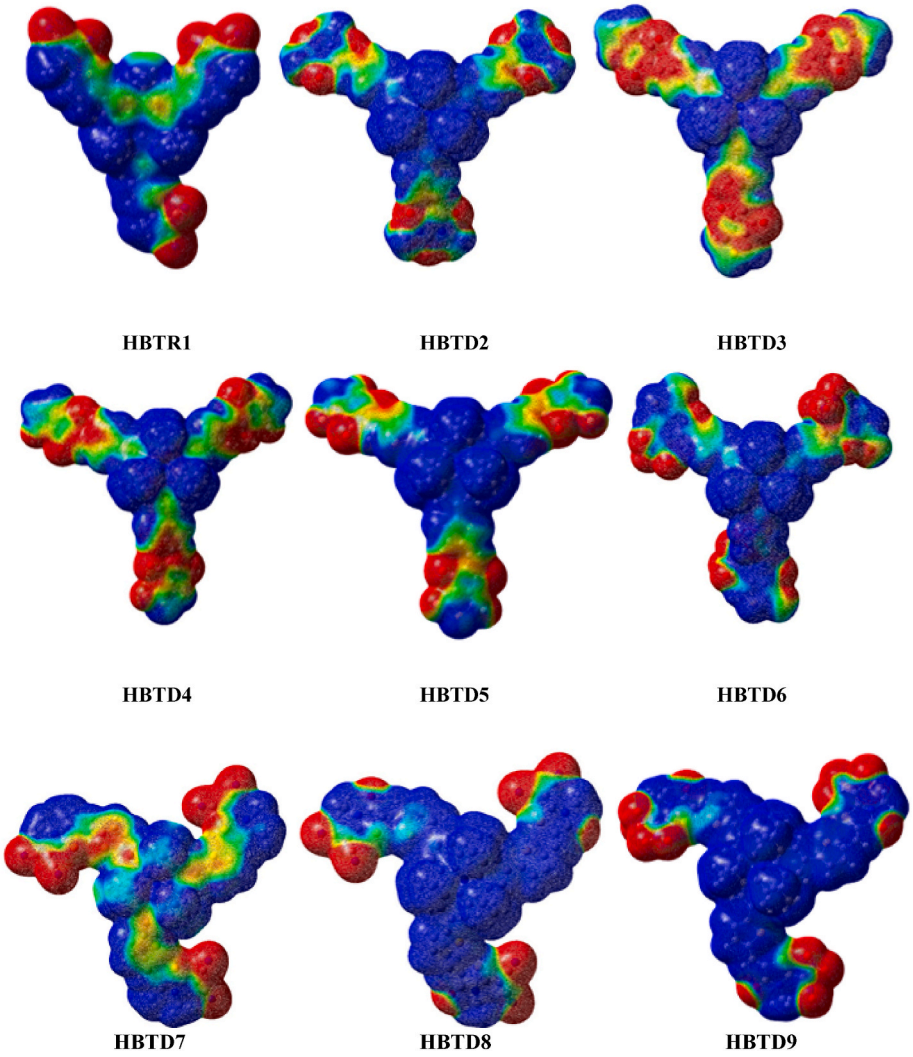

Fig. 9. Molecular electrostatic potential (MEP) diagram of **HBTR1** and **HBTD2-HBTD9**.

band gap among all entitled compounds was 2.183 eV, established for **HBTD9**, which exhibited the most bathochromic shift (λ_{max} = 659.175 nm) among the designed molecules. Additionally, all designed chromophores conferred a lower band gap (2.183–4.106 eV) contrary to the reference compound (4.179 eV). All designed molecules imparted a large excitation dissociation energy rate due to low binding energy (E_b = −0.337–1.407 eV) compared with **HBTR1** (E_b = 1.401 eV). Interestingly, an enhanced bathochromic shift in the absorption position of entitled compounds (λ_{max} = 429.933–659.175 nm) is recorded with lower transition energy (E = 0.750–2.140 eV). **HBTD9** has been demonstrated to have the highest potential for non-fullerene OSCs owing to the lowest band gap, large charge mobility, low oscillator strength, and low binding energy with good bathochromic absorption spectra among all studied molecules. All these findings show that all designed molecules (**HBTD2-HBTD9**) could be much better for manufacturing OSCs than the reference molecule (**HBTR1**) due to their enhanced photovoltaic behavior.

CRediT authorship contribution statement

Muhammad Khalid: Conceptualization, and design of the study, Writing – original draft, Writing – review & editing. **Ume Habiba Ishaque:** Conceptualization, and design of the study. **Muhammad Adnan Asghar:** Data curation. **Muhammad Adeel:** Data curation. **Mohammed Mujahid Alam:** Data curation. **Muhammad Imran:** Data curation. **Rabia Baby:** Data curation. **Ataualpa A.C. Braga:** Formal analysis. **Muhammad Fayyaz ur Rehman:** Conceptualization, and design of the study, Formal analysis. **Muhammad Safwan Akram:** Formal analysis, Writing – original draft, Writing – review & editing.

Declaration of competing interest

The authors declare that they have no known competing financial interests or personal relationships that could have appeared to influence the work reported in this paper.

Data availability

Data will be made available on request.

Acknowledgments

Dr. Muhammad Khalid gratefully acknowledges the financial support of HEC Pakistan (project no. 20–14703/NRPU/R&D/HEC/2021). A.A.C.B. (grant 2015/01491–3) is highly thankful to Fundação de Amparo á Pesquisa do Estado de São Paulo for the cooperation and financial assistance. A.A.C.B. (grant 312550/2020–0) also thanks to the Brazilian National Research Council (CNPq) for financial support and fellowship. This study was financed in part by the Coordenação de Aperfeiçoamento de Pessoal de Nivel Superior do Brasil (CAPES) Finance Code 001. M. M. A and M. I. express appreciation to the Deanship of Scientific Research at King Khalid University Saudi Arabia through a research groups program under grant number R.G.P. 2/59/1443.

Appendix A. Supplementary data

Supplementary data to this article can be found online at https://doi.org/10.1016/j.matchemphys.2023.127528.

References

[1] M. Panneerselvam, A. Kathiravan, R.V. Solomon, M. Jaccob, The role of π-linkers in tuning the optoelectronic properties of triphenylamine derivatives for solar cell applications–A DFT/TDDFT study, Phys. Chem. Chem. Phys. 19 (2017) 6153–6163.
[2] A.M. Makarieva, V.G. Gorshkov, B.-L. Li, Energy budget of the biosphere and civilization: rethinking environmental security of global renewable and non-renewable resources, Ecol. Complex. 5 (2008) 281–288.
[3] R. Avtar, et al., Exploring renewable energy resources using remote sensing and GIS—a review, Resources 8 (2019) 149.
[4] M. Salim, M. Rafiq, R.A. Khera, M. Arshad, J. Iqbal, Amplifying the photovoltaic properties of azaBODIPY core based small molecules by terminal acceptors modification for high performance organic solar cells: a DFT approach, Sol. Energy 233 (2022) 31–45.
[5] M. Khalid, et al., Efficient tuning of small acceptor chromophores with A1-π-A2-π-A1 configuration for high efficacy of organic solar cells via end group manipulation, J. Saudi Chem. Soc. 25 (2021), 101305.
[6] R. Hussain, et al., Efficient designing of triphenylamine-based hole transport materials with outstanding photovoltaic characteristics for organic solar cells, J. Mater. Sci. 56 (2021) 5113–5131.
[7] A. Polman, M. Knight, E.C. Garnett, B. Ehrler, W.C. Sinke, Photovoltaic materials: present efficiencies and future challenges, Science 352 (2016) aad4424.
[8] H. Hardianto, Utilization of solar power plant in Indonesia: a review, International Journal of Environment, Engineering and Education 1 (2019) 1–8.
[9] L. Meng, J. You, Y. Yang, Addressing the stability issue of perovskite solar cells for commercial applications, Nat. Commun. 9 (2018) 5265.
[10] R.A. Shehzad, et al., Designing of benzothiazole based non-fullerene acceptor (NFA) molecules for highly efficient organic solar cells, Computational and Theoretical Chemistry 1181 (2020), 112833.
[11] Z. Afzal, et al., Designing indenothiophene-based acceptor materials with efficient photovoltaic parameters for fullerene-free organic solar cells, J. Mol. Model. 26 (2020) 137.
[12] X. Xu, et al., Realizing over 13% efficiency in green-solvent-processed nonfullerene organic solar cells enabled by 1,3,4-thiadiazole-based wide-bandgap copolymers, Adv. Mater. 30 (2018), 1703973.
[13] D. Deng, et al., Fluorination-enabled optimal morphology leads to over 11% efficiency for inverted small-molecule organic solar cells, Nat. Commun. 7 (2016) 1–9.
[14] G. Yu, J. Gao, J.C. Hummelen, F. Wudl, A.J. Heeger, Polymer photovoltaic cells: enhanced efficiencies via a network of internal donor-acceptor heterojunctions, Science 270 (1995) 1789–1791.
[15] T. Liu, A. Troisi, What makes fullerene acceptors special as electron acceptors in organic solar cells and how to replace them, Adv. Mater. 25 (2013) 1038–1041.
[16] M. Adnan, M.Y. Mehboob, R. Hussain, Z. Irshad, Banana-shaped nonfullerene acceptor molecules for highly stable and efficient organic solar cells, Energy Fuel. 35 (2021) 11496–11506.
[17] A. Khalid, et al., Designing benzothiadiazole based non-fullerene acceptors with high open circuit voltage and higher LUMO level to increase the efficiency of organic solar cells, Optik 228 (2021), 166138.
[18] A. Mahmood, A. Tang, X. Wang, E. Zhou, First-principles theoretical designing of planar non-fullerene small molecular acceptors for organic solar cells: manipulation of noncovalent interactions, Phys. Chem. Chem. Phys. 21 (2019) 2128–2139.
[19] A. Mahmood, et al., A novel thiazole based acceptor for fullerene-free organic solar cells, Dyes Pigments 149 (2018) 470–474.
[20] C. Yan, et al., Non-fullerene acceptors for organic solar cells, Nat. Rev. Mater. 3 (2018) 1–19.
[21] J. Hou, O. Inganäs, R.H. Friend, F. Gao, Organic solar cells based on non-fullerene acceptors, Nat. Mater. 17 (2018) 119–128.
[22] Z. Liu, et al., Non-fullerene polymer acceptors based on perylene diimides in all-polymer solar cells, Sol. Energy Mater. Sol. Cell. 189 (2019) 103–117.
[23] Y. Huo, H.-L. Zhang, X. Zhan, Nonfullerene all-small-molecule organic solar cells, ACS Energy Lett. 4 (2019) 1241–1250.
[24] A. Venkateswararao, S.-W. Liu, K.-T. Wong, Organic polymeric and small molecular electron acceptors for organic solar cells, Mater. Sci. Eng. R Rep. 124 (2018) 1–57.
[25] W. Li, et al., The end-capped group effect on dithienosilole trimer based small molecules for efficient organic photovoltaics, J. Mater. Chem. C 4 (2016) 1972–1978.
[26] M. Weidelener, et al., Dithienopyrrole-based oligothiophenes for solution-processed organic solar cells, Chem. Commun. 49 (2013) 10865–10867.
[27] Y.N. Luponosov, et al., Star-shaped D–π–A oligothiophenes with a tris (2-methoxyphenyl) amine core and alkyldicyanovinyl groups: synthesis and physical and photovoltaic properties, J. Mater. Chem. C 4 (2016) 7061–7076.
[28] Y.N. Luponosov, et al., Effect of fused triphenylamine core in star-shaped donor-π-acceptor molecules on their physicochemical properties and performance in bulk heterojunction organic solar cells, Dyes Pigments 177 (2020), 108260.
[29] M.J. Frisch, F.R. Clemente, Gaussian 09, revision a. 01, mj frisch, gw trucks, hb schlegel, ge scuseria, ma robb, jr cheeseman, g. Scalmani, V. Barone, B. Mennucci, GA Petersson, H. Nakatsuji, M. Caricato, X. Li, HP Hratchian, AF Izmaylov, J. Bloino, G. Zhe 20–44 (2009).
[30] R.D. Dennington, T.A. Keith, J.M. Millam, GaussView 5.0, Gaussian. *Inc.*, Wallingford, 2008.
[31] B. Civalleri, C.M. Zicovich-Wilson, L. Valenzano, P. Ugliengo, B3LYP augmented with an empirical dispersion term (B3LYP-D*) as applied to molecular crystals, CrystEngComm 10 (2008) 405–410.
[32] T. Yanai, D.P. Tew, N.C. Handy, A new hybrid exchange–correlation functional using the Coulomb-attenuating method (CAM-B3LYP), Chem. Phys. Lett. 393 (2004) 51–57.

[33] C. Adamo, V. Barone, Exchange functionals with improved long-range behavior and adiabatic connection methods without adjustable parameters: the m PW and m PW1PW models, J. Chem. Phys. 108 (1998) 664–675.
[34] V.S. Bryantsev, M.S. Diallo, A.C. Van Duin, W.A. Goddard III, Evaluation of B3LYP, X3LYP, and M06-class density functionals for predicting the binding energies of neutral, protonated, and deprotonated water clusters, J. Chem. Theor. Comput. 5 (2009) 1016–1026.
[35] M. Walker, A.J. Harvey, A. Sen, C.E. Dessent, Performance of M06, M06-2X, and M06-HF density functionals for conformationally flexible anionic clusters: M06 functionals perform better than B3LYP for a model system with dispersion and ionic hydrogen-bonding interactions, J. Phys. Chem. 117 (2013) 12590–12600.
[36] F. Nimr Ajeel, A. Mohsin Khuodhair, S. Mahdi AbdulAlmohsin, Improvement of the optoelectronic properties of organic molecules for nanoelectronics and solar cells applications: via DFT-B3LYP investigations, Curr. Phys. Chem. 7 (2017) 39–46.
[37] S. Naqvi, A. Patra, Hole transport materials for perovskite solar cells: a computational study, Mater. Chem. Phys. 258 (2021), 123863.
[38] M.D. Ganji, M. Tajbakhsh, M. Kariminasab, H. Alinezhad, Tuning the LUMO level of organic photovoltaic solar cells by conjugately fusing graphene flake: a DFT-B3LYP study, Phys. E Low-dimens. Syst. Nanostruct. 81 (2016) 108–115.
[39] M.S. Abusaif, et al., New carbazole-based organic dyes with different acceptors for dye-sensitized solar cells: synthesis, characterization, dssc fabrications and density functional theory studies, J. Mol. Struct. 1225 (2021), 129297.
[40] A.L. Tenderholt, PyMOlyze: a Program to Analyze Quantum Chemistry Calculations, 2019. Preprint at, version 2.0.
[41] T. Lu, F. Multiwfn Chen, A multifunctional wavefunction analyzer, J. Comput. Chem. 33 (2012) 580–592.
[42] N.M. O'boyle, A.L. Tenderholt, K.M. Langner, Cclib: a library for package-independent computational chemistry algorithms, J. Comput. Chem. 29 (2008) 839–845.
[43] M.D. Hanwell, et al., Avogadro: an advanced semantic chemical editor, visualization, and analysis platform, J. Cheminf. 4 (2012) 1–17.
[44] Zhurko, G. A. & Zhurko, D. A. ChemCraft, version 1.6. URL: http://www.chemcraftprog.com (2009).
[45] A. Mahmood, Photovoltaic and charge transport behavior of diketopyrrolopyrrole based compounds with A–D–A–D–A skeleton, J. Cluster Sci. 30 (2019) 1123–1130.
[46] M.S. Ahmad, et al., Synthesis and XRD, FT-IR vibrational, UV–vis, and nonlinear optical exploration of novel tetra substituted imidazole derivatives: a synergistic experimental-computational analysis, J. Phys. Chem. Solid. 115 (2018) 265–276.
[47] M.R.S.A. Janjua, et al., Theoretical and conceptual framework to design efficient dye-sensitized solar cells (DSSCs): molecular engineering by DFT method, J. Cluster Sci. 32 (2021) 243–253.
[48] M.U. Khan, et al., Silico modeling of new "Y-Series"-based near-infrared sensitive non-fullerene acceptors for efficient organic solar cells, ACS Omega 5 (2020) 24125–24137.
[49] M.S. Nadeem, et al., Hydrothermally derived co, Ni co-doped ZnO nanorods; structural, optical, and morphological study, Opt. Mater. 111 (2021), 110606.
[50] M.S. Nadeem, et al., Enhancement in the photocatalytic and antimicrobial properties of ZnO nanoparticles by structural variations and energy bandgap tuning through Fe and Co co-doping, Ceram. Int. 47 (2021) 11109–11121.
[51] T. Munawar, et al., Rare earth metal co-doped Zn0· 9La0. 05M0. 05O (M= Yb, Sm, Nd) nanocrystals; energy gap tailoring, structural, photocatalytic and antibacterial studies, Mater. Sci. Semicond. Process. 122 (2021), 105485.
[52] T. Munawar, et al., Zn0. 9Ce0. 05M0. 05O (M= Er, Y, V) nanocrystals: structural and energy bandgap engineering of ZnO for enhancing photocatalytic and antibacterial activity, Ceram. Int. 46 (2020) 14369–14383.
[53] T. Munawar, et al., Structural, optical, electrical, and morphological studies of rGO anchored direct dual-Z-scheme ZnO-Sm2O3–Y2O3 heterostructured nanocomposite: an efficient photocatalyst under sunlight, Solid State Sci. 106 (2020), 106307.
[54] T. Munawar, et al., Multifunctional properties of Zn0· 9Mn0. 05M0. 05O (M= Al, Bi, Sr, Ag) nanocrystals-structural and optical study: enhance sunlight driven photocatalytic activity, Ceram. Int. 46 (2020) 22345–22366.
[55] M.U. Khan, et al., First theoretical framework of triphenylamine–dicyanovinylene-based nonlinear optical dyes: structural modification of π-linkers, J. Phys. Chem. C 122 (2018) 4009–4018.
[56] M.U. Khan, et al., First theoretical probe for efficient enhancement of nonlinear optical properties of quinacridone based compounds through various modifications, Chem. Phys. Lett. 715 (2019) 222–230.
[57] M.U. Khan, et al., Prediction of second-order nonlinear optical properties of D–π–A compounds containing novel fluorene derivatives: a promising route to giant hyperpolarizabilities, J. Cluster Sci. 30 (2019) 415–430.
[58] M.R.S.A. Janjua, et al., Effect of π-conjugation spacer (CC) on the first hyperpolarizabilities of polymeric chain containing polyoxometalate cluster as a side-chain pendant: a DFT study, Computational and Theoretical Chemistry 994 (2012) 34–40.
[59] M.N. Arshad, I. Shafiq, M. Khalid, A.M. Asiri, Exploration of the intriguing photovoltaic behavior for fused indacenodithiophene-based A–D–A conjugated systems: a DFT model study, ACS Omega 7 (2022) 11606–11617.
[60] M. Khalid, et al., Efficient tuning of small acceptor chromophores with A1-π-A2-π-A1 configuration for high efficacy of organic solar cells via end group manipulation, J. Saudi Chem. Soc. 25 (2021), 101305.
[61] J. Beheshtian, H. Soleymanabadi, A.A. Peyghan, Z. Bagheri, A DFT study on the functionalization of a BN nanosheet with PCX,(PC= phenyl carbamate, X= OCH3, CH3, NH2, NO2 and CN), Appl. Surf. Sci. 268 (2013) 436–441.
[62] M. Khalid, et al., First principles study of electronic and nonlinear optical properties of A–D–π–A and D–A–D–π–A configured compounds containing novel quinoline–carbazole derivatives, RSC Adv. 10 (2020) 22273–22283.
[63] A. Mahmood, M. HussainTahir, A. Irfan, B. Khalid, A.G. Al-Sehemi, Computational designing of triphenylamine dyes with broad and red-shifted absorption spectra for dye-sensitized solar cells using multi-thiophene rings in π-spacer, Bull. Kor. Chem. Soc. 36 (2015) 2615–2620.
[64] A. Mahmood, S.U.-D. Khan, U.A. Rana, Theoretical designing of novel heterocyclic azo dyes for dye sensitized solar cells, J. Comput. Electron. 13 (2014) 1033–1041.
[65] C. Sissa, et al., The effectiveness of essential-state models in the description of optical properties of branched push–pull chromophores, Phys. Chem. Chem. Phys. 12 (2010) 11715–11727.
[66] M. Ans, J. Iqbal, B. Eliasson, M.J. saif, K. Ayub, Opto-electronic properties of non-fullerene fused-undecacyclic electron acceptors for organic solar cells, Comput. Mater. Sci. 159 (2019) 150–159.
[67] M.N. Arshad, I. Shafiq, M. Khalid, A.M. Asiri, Exploration of the Intriguing Photovoltaic Behavior for Fused Indacenodithiophene-Based A–D–A Conjugated Systems: A DFT Model Study, ACS omega, 2022.
[68] S. Kraner, G. Prampolini, G. Cuniberti, Exciton binding energy in molecular triads, J. Phys. Chem. C 121 (2017) 17088–17095.
[69] A. Mahmood, A. Irfan, Effect of fluorination on exciton binding energy and electronic coupling in small molecule acceptors for organic solar cells, Computational and Theoretical Chemistry 1179 (2020), 112797.
[70] M.E. Köse, Evaluation of acceptor strength in thiophene coupled donor–acceptor chromophores for optimal design of organic photovoltaic materials, J. Phys. Chem. 116 (2012) 12503–12509.
[71] S. Kraner, R. Scholz, F. Plasser, C. Koerner, K. Leo, Exciton size and binding energy limitations in one-dimensional organic materials, J. Chem. Phys. 143 (2015), 244905.
[72] S.A. Siddique, et al., Efficient tuning of triphenylamine-based donor materials for high-efficiency organic solar cells, Computational and Theoretical Chemistry 1191 (2020), 113045.
[73] M. Ans, et al., Designing alkoxy-induced based high performance near infrared sensitive small molecule acceptors for organic solar cells, J. Mol. Liq. 305 (2020), 112829.
[74] M. Irfan, et al., Design of donor–acceptor–donor (D–A–D) type small molecule donor materials with efficient photovoltaic parameters, Int. J. Quant. Chem. 117 (2017), e25363.
[75] M. Ans, K. Ayub, S. Muhammad, J. Iqbal, Development of fullerene free acceptors molecules for organic solar cells: a step way forward toward efficient organic solar cells, Computational and Theoretical Chemistry 1161 (2019) 26–38.
[76] M. Azzouzi, T. Kirchartz, J. Nelson, Factors controlling open-circuit voltage losses in organic solar cells, Trends in Chemistry 1 (2019) 49–62.
[77] A. Khalid, et al., Designing benzothiadiazole based non-fullerene acceptors with high open circuit voltage and higher LUMO level to increase the efficiency of organic solar cells, Optik 228 (2021), 166138.
[78] M.U. Khan, et al., Molecular designing of high-performance 3D star-shaped electron acceptors containing a truxene core for nonfullerene organic solar cells, J. Phys. Org. Chem. 34 (2021) e4119.
[79] M.C. Scharber, et al., Design rules for donors in bulk-heterojunction solar cells—towards 10% energy-conversion efficiency, Adv. Mater. 18 (2006) 789–794.
[80] M.U. Khan, et al., Designing spirobifullerene core based three-dimensional cross shape acceptor materials with promising photovoltaic properties for high-efficiency organic solar cells, Int. J. Quant. Chem. 120 (2020), e26377.
[81] L. Liu, et al., Molecular electrostatic potential: a new tool to predict the lithiation process of organic battery materials, J. Phys. Chem. Lett. 9 (2018) 3573–3579.
[82] J.S. Murray, P. Politzer, The electrostatic potential: an overview, WIREs Computational Molecular Science 1 (2011) 153–163.
[83] G. Mahalakshmi, V. Balachandran, NBO, HOMO, LUMO analysis and vibrational spectra (FTIR and FT Raman) of 1-Amino 4-methylpiperazine using ab initio HF and DFT methods, Spectrochim. Acta Mol. Biomol. Spectrosc. 135 (2015) 321–334.
[84] M. Akram, et al., Highly efficient one pot palladium-catalyzed synthesis of 3, 5-bis (arylated) pyridines: comparative experimental and DFT studies, J. Mol. Struct. 1213 (2020), 128131.